Friction **11**(5): 685–703 (2023)
https://doi.org/10.1007/s40544-022-0643-4
ISSN 2223-7690
CN 10-1237/TH
RESEARCH ARTICLE

Wear monitoring method of water-lubricated polymer thrust bearing based on ultrasonic reflection coefficient amplitude spectrum

Changxiong NING[1], Fei HU[1], Wu OUYANG[2,3,*], Xinpin YAN[2,3], Dongling XU[4]

[1] *School of Naval Architecture, Ocean and Energy Power Engineering, Wuhan University of Technology, Wuhan 430063, China*

[2] *School of Transportation and Logistics Engineering, Wuhan University of Technology, Wuhan 430063, China*

[3] *Reliability Engineering Institute, National Engineering Research Center for Water Transport Safety, Wuhan 430063, China*

[4] *Alliance Manchester Business School, The University of Manchester, Manchester M156PB, UK*

Received: 26 August 2021 / Revised: 15 November 2021 / Accepted: 29 April 2022

Abstract: The water-lubricated thrust bearings of the marine rim-driven thruster (RDT) are usually composed of polymer composites, which are prone to serious wear under harsh working conditions. Ultrasonic is an excellent non-destructive monitoring technology, but polymer materials are characterized by viscoelasticity, heterogeneity, and large acoustic attenuation, making it challenging to extract ultrasonic echo signals. Therefore, this paper proposes a wear monitoring method based on the amplitude spectrum of the ultrasonic reflection coefficient. The effects of bearing parameters, objective function, and algorithm parameters on the identification results are simulated and analyzed. Taking the correlation coefficient and root mean square error as the matching parameters, the thickness, sound velocity, density, and attenuation factor of the bearing are inversed simultaneously by utilizing the differential evolution algorithm (DEA), and the wear measurement system is constructed. In order to verify the identification accuracy of this method, an accelerated wear test under heavy load was executed on a multi-functional vertical water lubrication test rig with poly-ether-ether-ketone (PEEK) fixed pad and stainless-steel thrust collar as the object. The thickness of pad was measured using the high-precision spiral micrometer and ultrasonic testing system, respectively. Ultimately, the results demonstrate that the thickness identification error of this method is approximately 1%, and *in-situ* monitoring ability will be realized in the future, which is of great significance to the life prediction of bearings.

Keywords: water-lubricated polymer thrust bearings; wear monitoring; ultrasonic reflection coefficient amplitude spectrum; parameter inversion; differential evolution

1 Introduction

The marine water-lubricated bearing primarily refers to the stern bearing and the thrust bearing of the marine propulsion system [1]. The former is generally installed in the stern tube or shaft frame to support the weight of the propeller and stern shaft, and the latter is currently and mainly used to carry the thrust force in the marine rim-driven thruster (RDT). Their common characteristics include: 1) The bearing is usually composed of polymer composites, such as rubber, Thordon, and Feroform; 2) the working condition is severe. On the one hand, the load is large, and the local specific pressure of water-lubricated stern bearing is 2–3 times the average specific pressure under the cantilever eccentric load of the propeller. The specific pressure of the water-lubricated thrust bearing of the megawatt level RDT exceeds 0.6 MPa,

* Corresponding author: Wu OUYANG, E-mail: ouyangw@whut.edu.cn

which is about 4 times the specific pressure of the water-lubricated stern bearing. On the other hand, the rotational speed is low, and the speed range is about 10–300 r/min. More importantly, it will be disturbed by the sediment in the water. The low viscosity of water causes the bearing capacity to be naturally weak. Under the factors of low speed, heavy load, impact, and sediment, the marine water-lubricated bearing is in a mixed lubrication state [2], which is prone to local contact friction [3] and wear [4], causing abnormal noise [5, 6] and shaft vibration [7, 8].

Wear test is a vital research method for designing material and bearing tribological performance. Wear measurement is divided into *non-in-situ* and *in-situ* measurements depending on whether the original conditions of the system changed or whether the measurement object is isolated from the original system. Common *non-in-situ* measurement methods include methods for weighing, wear scar measurement, and worn surface observation. The weighing method uses a high-precision balance to measure the weight before and after wear [9]. It is suitable for gauging the amount of wear in a small test block, but it is unable to generate detailed information on the measured object. Qu and Truhan [10] adopted the single-track analysis method to quantify the size of bearing wear scars, which is beneficial for analyzing the wear mechanism. However, the measured object must be disassembled. Bhushan and Lowry [11] produced a nano-scratch array at the center of the head sample surface using a commercial nanoindenter. They determined the scratch depths before and after running against magnetic tapes as a direct measure of wear on the head surface through an atomic force microscope. Moreover, this technology had high measurement accuracy.

The *in-situ* measurement method directly installs the test system in the tested object without affecting the normal operation of the equipment as much as possible, which has higher requirements for installation conditions. Radioactive measurement [12] and ferrography measurement [13] are two common *in-situ* wear measurement techniques. With the development of image processing technology, several new wear measurement methods have appeared in recent years [14]. Based on digital image processing technology, Zhang et al. [15] separated the wear area from the worn image captured by the CCD camera under the 100× optical system. The worn three-dimensional (3D) surface was reconstructed using an algorithm, and the wear width and the wear loss were extracted. By employing the radioisotope tracing technique, the innovative research of Warner et al. [16] measured the local backside wear on ultrahigh molecular weight polyethylene (UHMWPE) tibial inserts in low-contact stress (LCS) mobile bearing knee prostheses. Yuan et al. [17] put forward morphology to analyze wear particle information, such as wear particle contour, shape, fractal dimension, and color. In recent years, scholars introduced intelligent algorithms like transfer learning, support vector machine [18] and belief-rule-based expert, and evidential reasoning rule [19] into the identification of wear particles and faults. However, these methods can only obtain qualitative information on the wear. Then, Kang et al. [20] designed a set of rolling bearing wear testing systems composed of the indicator needle installed on the upper plate of the bearing. Meanwhile, the corresponding scale of the pointer, which is mounted on the lower plate of the bearing, is read at regular intervals to identify the distance between the upper and lower plates of the bearing and to calculate the amount of wear. However, the test accuracy is deemed insufficient due to the low accuracy of the scale and the greater influence of the installation and operating environment.

The essence of linear wear measurement is a distance measurement. As a non-intrusive measurement technology, the straight-line propagation characteristics of ultrasound retain the advantages of optical methods. Its strong penetrating ability compensates for the lack of transparency required by optical methods and has the potential for *in-situ* wear measurement. Long and Rack [21] adopted the ultrasonic method to measure the amount of wear of metal materials. It proved that the ultrasonic time-of-flight method can be used for the continuous measurement of wear *in situ*. Then, Ahn and Kim [22] evaluated the feasibility of an ultrasonic technique through the pulse-echo method of normal incident compressional waves to worn surface condition and subsurface damage in sliding friction progress. Abu-Zahra and Yu [23] utilized the discrete wavelet transform (DWT) of ultrasound waves to measure the gradual wear of carbide inserts

during turning operations. The main feature of this research is the introduction of neural networks to analyze signals.

Currently, ultrasonic wear measurement is for metal materials with uniform materials. Generally, the water-lubricated bearings are made of polymer composite materials (polymer base materials, reinforcing agents, and impurities), such as nitrile rubber, Feroform, or Thordon, where ultrasonic waves undergo complex refraction, reflection, scattering, and other propagation phenomena. Acoustic characteristic parameters vary significantly, and there are numerous influencing factors, which are difficult to obtain accurately, resulting in low recognition accuracy for the thickness of non-uniform material.

Zhao et al. [24] proposed a method based on the ultrasonic reflection coefficient amplitude spectrum (URCAS) to inverse the coating thickness and sound velocity. Their findings demonstrated that the relative error of the identification of homogeneous and heterogeneous coatings was less than 10%. Ma et al. [25] recommended a method for characterizing the surface roughness and thickness of non-uniform coatings according to the Ultrasonic Reflection Coefficient Phase Spectroscopy (URCPS). The relative error between the calculated results of the WC–Ni coating and the scanning electron microscope (SEM) observation results was less than 11%. Balasubramaniam and Rao [26] used genetic algorithm-based inversion technology to calculate the stiffness characteristics of fiber- reinforced composites based on ultrasonic volume waves. Their approach was more robust and global than traditional gradient-based methods. At present, the inversion technology based on the reflection coefficient spectrum has been utilized for the characterization of the physical parameters of non-metallic coatings. Whether it can be applied to the wear measurement of polymer bearings remains inconclusive, and the application of intelligent algorithms in ultrasonic parameter inversion necessitates further investigation.

Therefore, this paper establishes the wear identification model of polymer bearings based on ultrasonic. It also deduced the relationship among the acoustic velocity, thickness, density, attenuation factor of polymer bearings, and the URCAS. Additionally, the correlation coefficient and root mean square error are used as the objective function, and four parameters are simultaneously inversed by combining the differential evolution algorithm (DEA), addressing the problem that the acoustic characteristic parameters of polymer bearings are difficult to obtain. Then, PEEK bearing and stainless-steel thrust collar are selected as the objects, and a heavy load accelerated wear test is performed on the vertical water-lubricated bearing test rig. In order to verify the test accuracy of the method, the disassembled pads are measured using the ultrasonic probe and high-precision spiral micrometer every hour. Finally, the accuracy of different ultrasonic calculation methods and intelligent algorithms in thickness identification are compared.

2 Bearing wear monitoring theory

2.1 Ultrasonic propagation model

The fundamental idea behind the ultrasonic-based bearing wear monitoring method is obtaining linear wear amount by identifying the thickness of polymer bearings pre- and post-wear. Ultrasonic signals could be reflected and transmitted on the surface of the layered structure, and materials with distinct properties play the role of linear filtering in this process. Moreover, the reflection coefficient of the reflected signal of the layered structure can be used to describe physical and geometric features. Figure 1 shows the model of ultrasonic signal propagation in the bearing, and this model simplifies the bearing into a homogeneous, layered material with a smooth interface. The medium I is a delayed block that can better couple the acoustic energy into the polymer material. Medium II is a layered polymer material, and medium

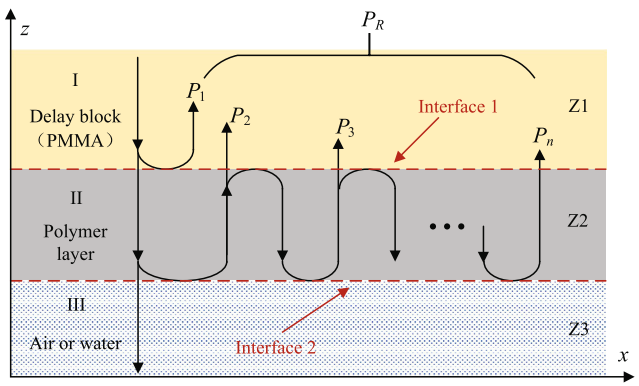

Fig. 1 Schematic diagram of vertical incidence of ultrasonic to a three-layer structure.

III is air or water. The acoustic impedance of the three is $Z1$, $Z2$, and $Z3$, respectively, where it is numerically equal to the medium density multiplied by the sound velocity.

Assuming the sound pressure is 1, the ultrasonic pulse wave with frequency f is vertically incident into the three-layer medium along the negative direction of the z-axis (Fig. 1). The received reflected wave can be expressed as [24]:

$$\begin{cases} P_1 = r_{12} \\ P_2 = r_{23}t_{12}t_{21}\exp(2ik_{2z}d) \\ P_3 = r_{23}^2 t_{12}r_{21}t_{21}\exp(4ik_{2z}d) \\ \cdots\cdots \\ P_n = r_{23}^n t_{12}r_{21}^{n-1}t_{21}\exp[2(n-1)ik_{2z}d],\ k_{2z} = \dfrac{2\pi f}{c_2} + i\alpha \end{cases} \tag{1}$$

where P_1 is the reflection echo of the upper interface of the polymer layer; P_2 is the sound wave transmitted into the polymer layer, reflected once on the lower interface, and transmitted out of the upper interface; and P_3 is the sound wave transmitted into the polymer layer, reflected twice on the lower interface, and transmitted out of the upper interface. Then, P_n is the acoustic wave transmitted into the polymer layer, reflected n times on the lower interface, and transmitted out of the upper interface. Next, r_{12} and r_{23} are the acoustic pressure reflection coefficients of interfaces 1 and 2, respectively, t_{12} and t_{21} are acoustic pressure transmission coefficients in different directions at interface 1, n is the number of reflected echoes, d and c_2 are thickness and longitudinal wave velocity of the polymer layer, respectively, α is the attenuation coefficient of the polymer layer, k_{2z} is the wave number along the z-direction in the polymer layer, and $\exp(2ik_{2z}d)$ is the phase change after the sound wave reciprocates through the polymer layer once.

Due to the interfacial reflection and transmission loss of the polymer layer, as well as the absorption and diffusion attenuation inside the material, the signal attenuation is severe during the propagation of the ultrasonic wave. Only the first echoes on the upper and lower surfaces of the polymer layer can be received. Therefore, the reflection coefficient R of the polymer layer is

$$R = \frac{P_1 + P_2}{P_1} = \frac{r_{12} + t_{12}r_{23}t_{21}\exp(-2\alpha d)\cos\left(\dfrac{4\pi fd}{c_2}\right)}{r_{12}} + i\frac{t_{12}r_{23}t_{21}\exp(-2\alpha d)\sin\left(\dfrac{4\pi fd}{c_2}\right)}{r_{12}} \tag{2}$$

The acoustic pressure reflection coefficient R is a complex number, and its module is a function of frequency, called the URCAS. The expression is

$$R(f) = \sqrt{\left\{\left[r_{12}^2 + 2r_{12}r_{23}(1-r_{12}^2)\exp(-2\alpha d)\cos\left(\frac{4\pi fd}{c_2}\right) + r_{23}^2(1-r_{12}^2)^2\exp(-4\alpha d)\right] \Big/ r_{12}^2\right\}} \tag{3}$$

The attenuation coefficient of the polymer layer is

$$\alpha(f) = \frac{1}{2d}\ln\left[\frac{(1-r_{12}^2)r_{23}A_1(f)}{r_{12}A_2(f)}\right] = \frac{1}{2d}\ln\left[w\cdot\frac{A_1(f)}{A_2(f)}\right] \tag{4}$$

where $A_1(f)$ and $A_2(f)$ are amplitude spectrums of reflection echo at the upper and lower interfaces of the polymer layer, respectively. The attenuation factor w is introduced to facilitate subsequent calculations.

At certain frequencies, the echoes of the upper and lower interfaces P_1 and P_2 could interfere, which is reflected in the amplitude spectrum as the maximum or minimum point with the same frequency interval. The thickness of the polymer layer can be expressed by the frequency interval Δf and the acoustic velocity, which is known as the spectral resonance (SR) method:

$$d = \frac{c_2}{2\Delta f} \tag{5}$$

When the acoustic attenuation of polymer bearings is large and the echo signal-to-noise ratio is low, it is difficult to derive an accurate acoustic velocity or thickness according to the characteristics of the frequency domain's extreme points. Figure 2, in which v is the linear velocity of the thrust collar and W is the axial load, illustrates that during the production process, other components are added to enhance the performance. The temperature distribution during the operation is not uniform, and the propagation speed of sound waves is challenging to determine. At the same

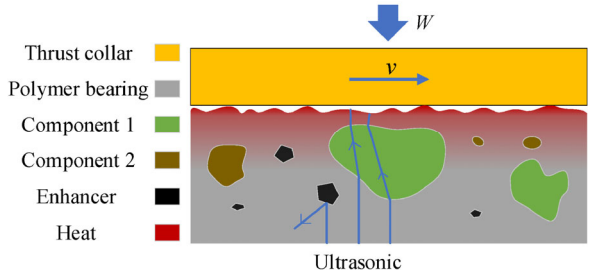

Fig. 2 Complex propagation phenomenon of ultrasonic waves in the non-uniform polymer bearing.

time, the bearing has thermoelastic deformation, and the geometric parameters and physical parameters are variable. Therefore, it is necessary to develop a method that can simultaneously solve multiple parameters of polymer bearings to meet the requirements of wear monitoring.

Equation (3) shows that the URCAS is a function of the sound velocity, thickness, density, attenuation coefficient, and other parameters of the polymer layer. The propagation process of ultrasonic waves in polymer bearing is assumed to be a black box system. Using this formula, a series of mapping matrices between medium parameters and URCAS are constructed. The appropriate objective function is selected to characterize the similarity between the measured echo information and the theoretical calculation. Subsequently, the parameter inversion problem is transformed into an extremum optimization problem.

This paper selects the correlation coefficient and root mean square error as the objective functions to measure the similarity between the theoretical and measured URCAS. The Pearson correlation coefficient (Pcc) matching method has been applied in other fields, such as parameter inversion, reflecting the similarity of the variation trend of the two data sets. The Pcc expression can be obtained by substituting the theoretical URCAS and the measured URCAS in Eq. (3):

$$\begin{aligned} r_p(c_2,d,p,w) = & \left\{\sum_{i=1}^{N}\left[R(f;c_2,d,p,w)-\overline{R(f;c_2,d,p,w)}\right]\cdot\right. \\ & \left.\left[R(f;c_2,d,p,w)^*-\overline{R(f;c_2,d,p,w)^*}\right]\right\} \Big/ \\ & \left\{\sqrt{\sum_{i=1}^{N}\left[R(f;c_2,d,p,w)-\overline{R(f;c_2,d,p,w)}\right]^2}\cdot\right. \\ & \left.\sqrt{\sum_{i=1}^{N}\left[R(f;c_2,d,p,w)^*-\overline{R(f;c_2,d,p,w)^*}\right]^2}\right\} \end{aligned} \tag{6}$$

where N is the number of data points in the frequency domain after the fast Fourier transform (FFT) transform of the time domain signal, the subscript i is the i-th frequency value. Then, $R(f;c_2,d,p,w)$ and $R(f;c_2,d,p,w)^*$ are the measured and theoretical URCAS in the effective frequency band, respectively. In addition, $\overline{R(f;c_2,d,p,w)}$ and $\overline{R(f;c_2,d,p,w)^*}$ are the arithmetic means of the measured and theoretical URCAS in the effective frequency band, respectively.

Since only the Pcc is used as the objective function without considering the difference in amplitude, falling into the minimum point in the calculation process is highly probable. Thus, the root mean square error (RMSE) is introduced as the second constraint, which reflects the numerical consistency of the two data sets. By substituting the measured value $R(f;c_2,d,p,w)$ and theoretical value $R(f;c_2,d,p,w)^*$ of URCAS, the RMSE expression is generated as

$$\mathrm{RMSE}=\sqrt{\frac{1}{N}\sum_{i=1}^{N}\left[R(f;c_2,d,p,w)-R(f;c_2,d,p,w)^*\right]^2} \tag{7}$$

When the Pcc is the largest and the RMSE is the smallest, the similarity between the theoretical and measured URCAS is the largest. Additionally, the independent variable corresponding to the objective function is the parameter value of the polymer bearing.

2.2 Differential evolutionary algorithm

DEA is an algorithm based on population evolution [27]. Its advantages include having a simple structure, few adjustment parameters, and strong robustness. Essentially, it is a greedy genetic algorithm with the idea of preserving superiority based on real number coding. Firstly, DEA randomly generates a population $\{X_{1,g}, X_{2,g}, \cdots, X_{NP,g}\}$ containing NP feasible solutions. The individual $X_{j,g}=\left(x_{1,g}^j, x_{2,g}^j, \cdots, x_{D,g}^j\right)$ is used to describe the problem solution, where D is the dimensionality of the optimization variable, and g is the evolutionary epoch. Each individual is uniformly and randomly determined within the range $[X_{\min}, X_{\max}]$, where $X_{\min}=\left(x_{\min}^1, x_{\min}^2, \cdots, x_{\min}^D\right)$, $X_{\max}=\left(x_{\max}^1, x_{\max}^2, \cdots, x_{\max}^D\right)$. This series of random individuals constitutes the initial population:

$$x_i^j = x_{\min}^j + \mathrm{rand}(0,1)\cdot(x_{\max}^j - x_{\min}^j), j\in[1,D] \tag{8}$$

where rand (0,1) is a real number uniformly randomly determined between 0 and 1.

The DEA realizes individual mutation through differential strategy, which is an important sign that distinguishes it from the genetic algorithm. The classic mutation strategy is randomly selecting two different individuals in the population and then scaling their vector difference to perform vector synthesis with the individual to be mutated. The generated mutation vector $V_{i,g}$ is

$$V_{i,g} = X_{a,g} + F \cdot (X_{b,g} - X_{c,g}), \quad a \neq b \neq c \neq i \tag{9}$$

where $X_{a,g}$, $X_{b,g}$, and $X_{c,g}$ are three randomly selected individuals in the population, and F is the scaling factor.

To improve the diversity of the population, the DEA introduces a crossover operation, so that at least one component in the test vector comes from the mutation vector:

$$U_{i,g+1} = \begin{cases} V_{i,g}^{j}, & \text{if } (\text{rand}^{j}(0,1) \leq \text{CR}) \text{ or } (j = j_{\text{rand}}) \\ X_{i,g}^{j}, & \text{otherwise} \end{cases} \tag{10}$$

where $\text{rand}^{j}(0,1)$ is the uniform random number calculated for the j-th time between 0 and 1. The CR is the crossover probability within the range of [0,1]. Index j_{rand} is a randomly selected dimension. It ensures that the test vector $U_{i,g+1}$ gets at least one element from $V_{i,g}$, known as the binomial uniform crossover.

The individuals generated through mutation and crossover operations are compared with their parent individuals, and the better-performing ones enter the next-generation population:

$$X_{i,g+1} = \begin{cases} U_{i,g+1}, & \text{if } f(U_{i,g+1}) < f(X_{i,g}) \\ X_{i,g}, & \text{otherwise} \end{cases}, \quad i = 1,2,\cdots,\text{NP} \tag{11}$$

After mutation, crossover, and selection operations, new individuals can be generated in that form and the same number for the next-generation population. The previous-generation population will continue to circulate until the termination condition is met.

In summary, Fig. 3 presents the flowchart of the bearings wear monitoring method based on URCAS combined with DEA. The difference between the

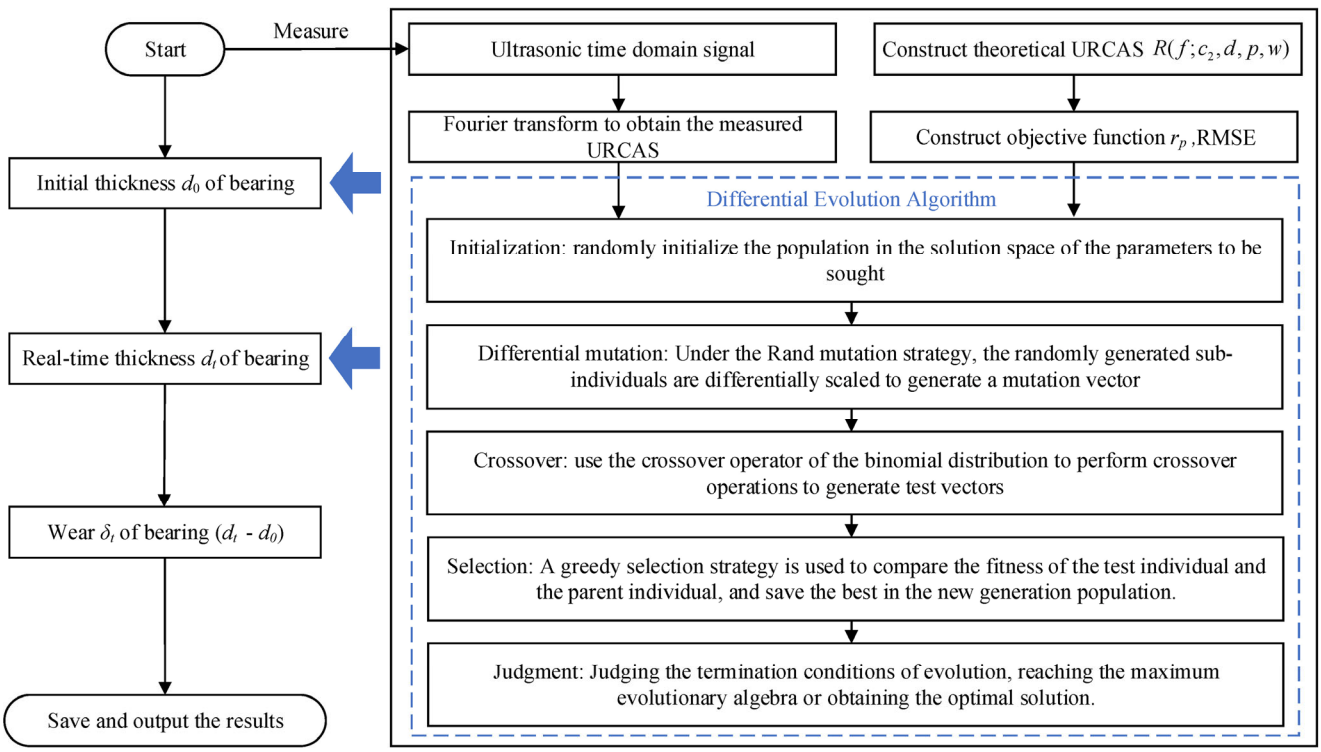

Fig. 3 Flow chart of polymer bearing wear monitoring method.

real-time thickness d_t at the measuring point of the ultrasonic probe and the thickness d_0 before wear is the value of wear amount δ_t.

3 Simulation

3.1 Influence of bearing parameters on URCAS

According to Eqs. (3) and (4), URCAS is a function of the acoustic parameters and geometric characteristics of each medium layer. When the acoustic parameters of the medium other than the polymer layer are known, URCAS is solely related to the acoustic velocity, thickness, density, and attenuation factor of the polymer. As a result, the influence of the change of polymer parameters on URCAS in the effective frequency band can be discussed, where the acoustic velocity and density satisfy the coupling relationship expressed as

$$c_2 = \sqrt{\frac{E(1-\mu)}{\rho(1+\mu)(1-2\mu)}} \tag{13}$$

where E is the elastic modulus of the medium, μ is the Poisson's ratio of the medium, and ρ is the density of the medium. When the change of acoustic velocity is discussed separately, the density will also change according to this formula, and vice versa.

As shown in Fig. 4, the change of acoustic velocity near the frequency of 2.75 MHz fundamentally does not cause a change in amplitude. When the frequency is lower than 2.75 MHz, the increase of acoustic velocity will make the position of amplitude spectrum resonance point shift to low frequency, and a decrease in acoustic velocity will make it to high frequency. When the frequency is higher than 2.75 MHz, the deviation of the amplitude spectrum is completely the opposite. At the same time, the correlation coefficient (r_p) between the amplitude spectrum and theoretical true value will decrease to 0.834, and RMSE will rise to 0.931 because of the 10% increase in acoustic velocity. The correlation coefficient will decrease to 0.819, and RMSE will increase to 0.975 because of the 10% decrease in the acoustic velocity. The spectrum offset caused by the decrease of acoustic velocity is slightly larger than that caused by the increase of acoustic velocity. Moreover, the correlation coefficient must exceed 0.834, and RMSE must be less than 0.931 to maintain the inversion error of acoustic velocity at less than 10%.

Figure 5 portrays that the change of thickness near the frequency of 2.45 MHz essentially does not cause the change in amplitude. On the one hand, when the frequency is lower than 2.45 MHz, the increase of thickness will make the position of the amplitude spectrum resonance point shift to high frequency, and a decrease in the thickness will make it shift to low frequency. On the other hand, when the frequency is larger than 2.45 MHz, the deviation of the amplitude spectrum is completely the opposite. Meanwhile, the correlation coefficient will decrease to 0.795, and RMSE will increase to 1.037 because of the 10%

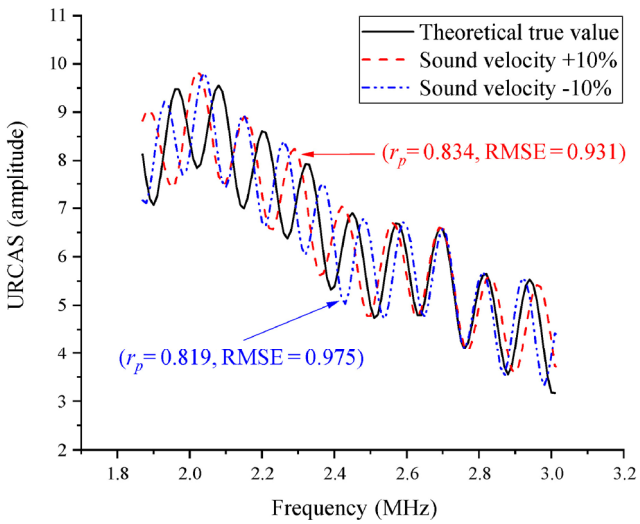

Fig. 4 Effect of acoustic velocity fluctuation ± 10% on URCAS.

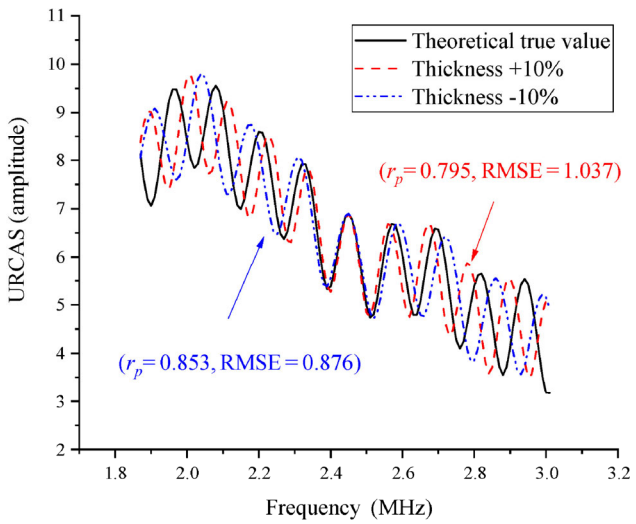

Fig. 5 Effect of thickness fluctuation ± 10% on URCAS.

increase in thickness. In contrast, the correlation coefficient will decrease to 0.853, and RMSE will increase to 0.876 because of the 10% decrease in thickness. Overall, the spectrum offset caused by the increase in thickness is slightly larger than that caused by the decrease.

As shown in Fig. 6, the increase in density shifts the amplitude spectrum to low frequency in the effective frequency band. The decrease of density near the frequency of 2.6 MHz does not cause a change in the amplitude. When the frequency is lower than 2.6 MHz, the resonance point of the amplitude spectrum shifts to low frequency, and it shifts to high frequency when the frequency is higher than 2.6 MHz. At the same time, the correlation coefficient will decrease to 0.725, and RMSE will increase to 1.193 because of the 10% increase in density. The correlation coefficient will decrease to 0.968, and RMSE will increase to 0.411 because of the 10% decrease in the density. The spectrum deviation caused by the increase in density is significantly larger than that caused by the decrease in density, indicating that the sensitivity of identifying the amplitude spectrum lower than the true value of the density is relatively low. In this case, the correlation coefficient must be more than 0.968, and RMSE should be less than 0.411 to maintain the inversion error of density at a value less than 10%.

As shown in Fig. 7, the increase or decrease in the attenuation factor will result in the overall upward or downward migration of the amplitude spectrum.

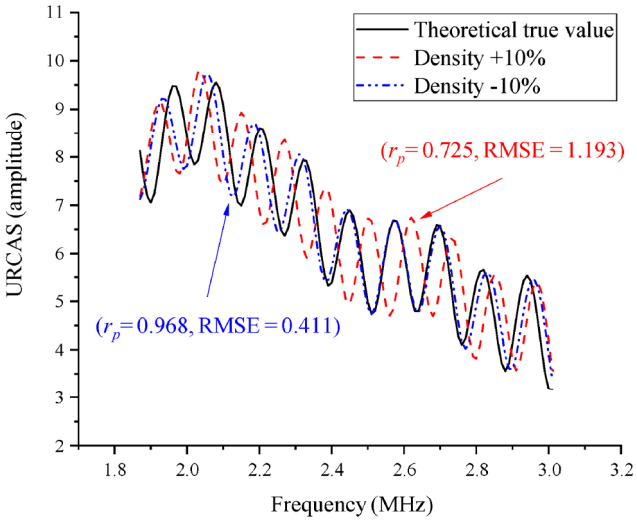

Fig. 6 Effect of density fluctuation ± 10% on URCAS.

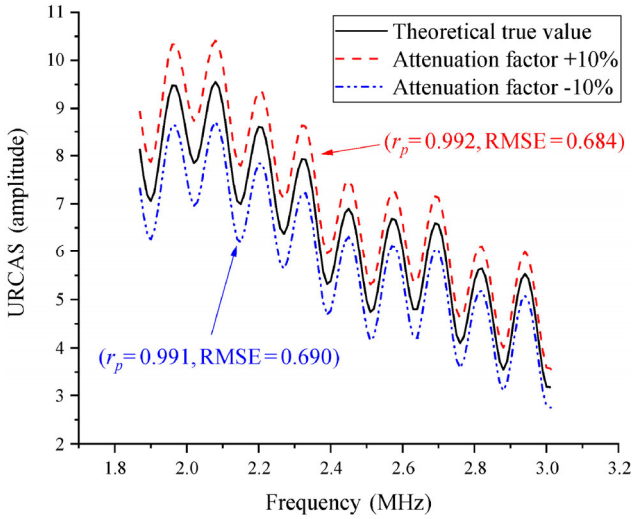

Fig. 7 Effect of attenuation factor fluctuation ± 10% on URCAS.

Meanwhile, the change in the attenuation factor principally does not alter the correlation coefficient between the amplitude spectrum and the theoretical true value, which is greater than 0.99. The increase and decrease in the attenuation factor will increase RMSE to 0.684 and 0.690, respectively. In this event, the correlation coefficient as the objective function cannot identify the change of attenuation factor and could result in a large error. So, RMSE is introduced as a constraint.

In summary, to ensure that the inversion error of the four parameters are less than 10%, the correlation coefficient between the calculation result and the theoretical value needs to be greater than 0.991, and RMSE is less than 0.411.

3.2 Influence of objective function on identification results

The objective function is used to characterize the matching degree between the observed value and the calculated value. Also, it is the fitness function in the intelligent optimization algorithm that is one of the most important indicators of whether the model represents the actual system. Pcc has been widely adopted as an objective function in inversion problems. Moreover, RMSE is introduced to explore the influence of different objective functions on the inversion results. The effects of the single objective function and the dual objective function on the results are discussed, respectively. The evaluation indexes include the mean

(M) and standard deviation (SD) of 10 calculations and the similarity between the calculated amplitude spectrum and the measured spectrum.

As shown in Fig. 8, the M of the inversion sound velocity of the Pcc significantly deviates from the true value, with a relative error of 1.50%, followed by RMSE. The dual objective function has the smallest relative errors, which is 0.75%. The SD of RMSE has the smallest value at 25.92 m·s^{-1}, followed by the dual objective function at 30.39 m·s^{-1}. The SD of Pcc is the largest at 34.02 m·s^{-1}.

As depicted in Fig. 9, the M of the inversion thickness of Pcc is closest to the true value, with an absolute error of 15 μm. The mean thickness of the dual objective function has an absolute error of 24 μm. Meanwhile, the mean thickness of RMSE deviates from the true value at a relatively large value, with an absolute error of 54 μm. The SD of Pcc has the smallest value at 44.89 μm, followed by the dual objective function at 55.85 μm. Then, the SD of RMSE is the largest at 68.78 μm.

As illustrated in Fig. 10, the M inversion density of Pcc considerably deviates from the true value, and the relative error is 1.81%. The M density of the dual objective function is slightly larger than the true value, and the relative error is 0.47%. Given these findings, the RMSE results are fundamentally consistent with the true value. Moreover, the SD of Pcc has the smallest value at 0.006 g·cm^{-3}, followed by the dual objective function at 0.014 g·cm^{-3}. The SD of RMSE is the largest, which was 0.019 g·cm^{-3}.

As shown in Fig. 11, the M of inversion attenuation factor of the RMSE and the Pcc are respectively larger and smaller than the true value, with relative errors

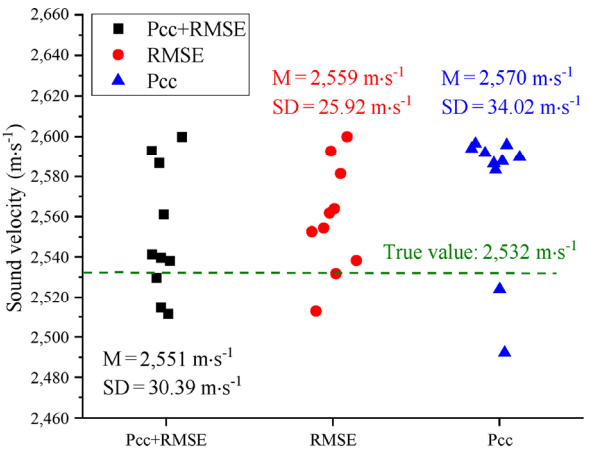

Fig. 8 Effect of different objective functions on the inversion results of acoustic velocity.

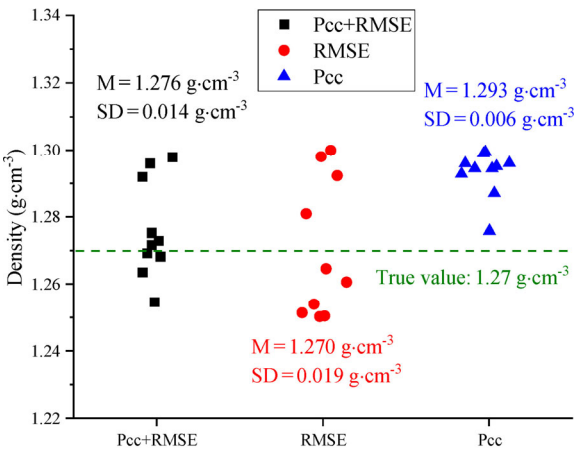

Fig. 10 Effect of different objective functions on the inversion results of density.

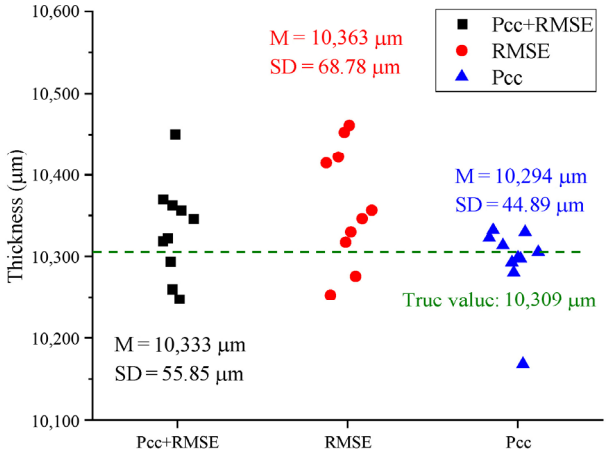

Fig. 9 Effect of different objective functions on the inversion results of thickness.

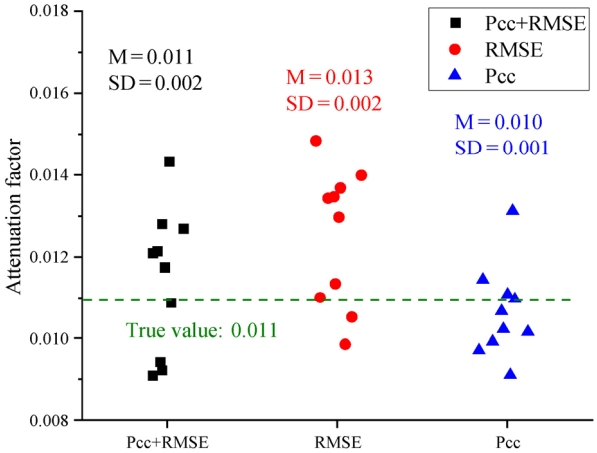

Fig. 11 Effect of different objective functions on the inversion results of the attenuation factor.

of 18.18% and 9.09%. The inversion results of the dual objective function are almost consistent with the true value. The SD of Pcc is the smallest, which is 0.001, and the SDs of dual objective function and RMSE are both 0.002.

Figure 12 demonstrates the calculation differences among the various objective functions. The correlation coefficients in the three cases can reach 0.998, but the RMSE is larger when the Pcc is the objective function. The curve shows a slight upward shift, which is because there is no constraint on the calculation value, and it is easy to fall into the minimum value near the optimal solution. Moreover, RMSE is consistent with the identification results of the dual objective function, and the matching degree is the highest.

In summary, Pcc, as the objective function, has the smallest SD of the inversion result. However, the M inversion parameters, other than the thickness, have larger relative errors. As the objective function, RMSE has the largest SD of the inversion result, but the error of the inversion mean is less than that of the correlation coefficient. When the two objective functions are combined, the M inversion results are closer to the true value, and the SD is smaller than that of the single RMSE as the objective function. Simultaneously, the calculation time is slightly reduced. Therefore, Pcc and RMSE are utilized as the objective functions of the optimization algorithm, and the 3D image of the sound velocity and thickness solution space is simulated (Fig. 13).

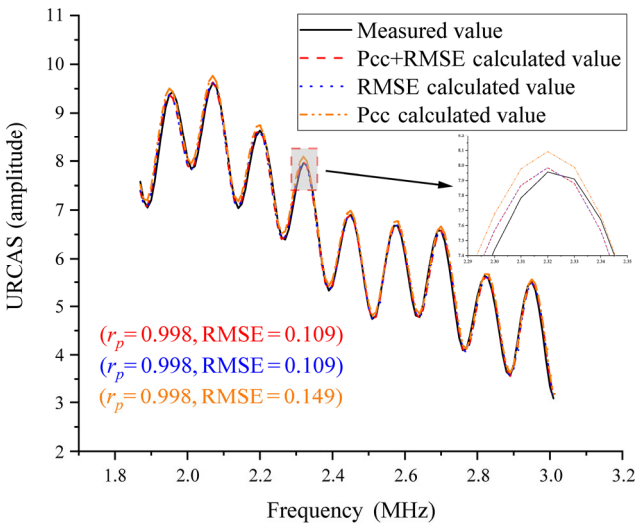

Fig. 12 Effect of different objective functions on URCAS.

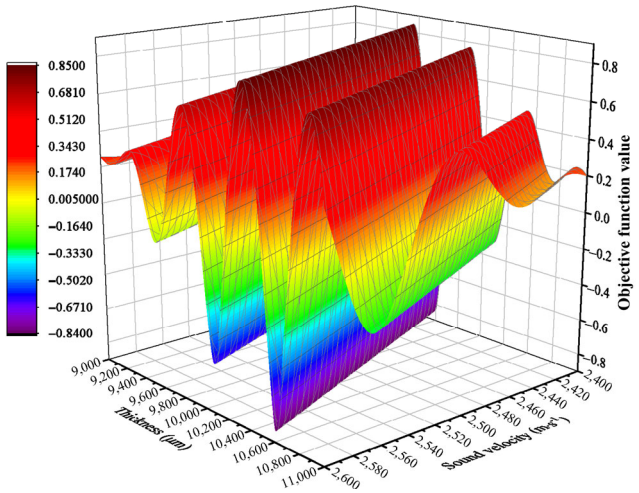

Fig. 13 Solution space of the dual objective function with respect to sound velocity and thickness.

3.3 Influence of algorithm parameters on identification results

The five settable parameters in DEA are evolution epochs, population size, weight factor, crossover rate, and mutation strategy. Usually, the latter three use the default parameters of the algorithm, and the evolution epochs and population size are the main adjustment parameters. Therefore, this paper solely discusses the influences of different evolution epochs and population sizes on the calculation time and identification results. The criterion is that the mean thickness is, as much as possible, close to the true value, the SD is as small as possible, and the calculation time is as short as possible.

As portrayed in Fig. 14, by changing the evolutionary epochs to discuss its influence on the convergence of the fitness function, the population size defaults to 50. The fitness function (line chart) does not converge to the minimum after the 50th and the 100th generations of evolution. Starting from the 150th generation, the fitness function can converge to the minimum. Essentially, with the increase of evolutionary epochs, the calculation time (bar chart) increases linearly. When the inversion results of other medium parameters are accurate, the focus is on the thickness accuracy. As shown in Fig. 15, the thickness results obtained by different evolutionary epochs fluctuate above and below the true value, and the relative error of the mean thickness is less than 1%. No evident linear relationship exists between the increase in the

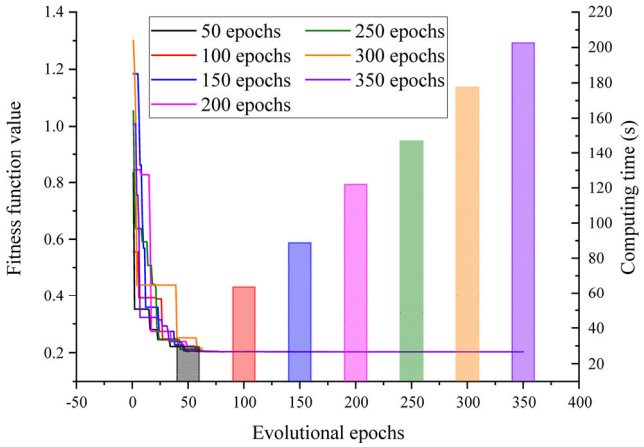

Fig. 14 Effect of different evolution epochs on the convergence of fitness function.

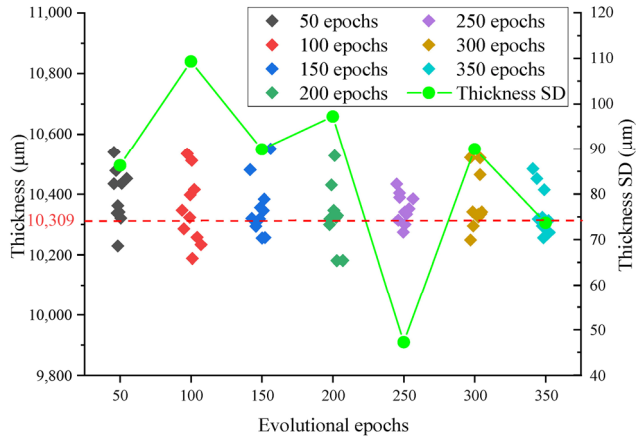

Fig. 15 Effect of different evolution epochs on thickness inversion results.

evolutionary epochs and the calculation accuracy. Considering the SD of the inversion thickness, the SD of 250 generations is the smallest, which is 47 μm, and the inversion thickness results are the most concentrated. Therefore, 250 generations are selected as the optimal algorithm parameters.

As shown in Fig. 16, the evolutionary epoch selects 250 generations and changes the population size to explore its impact on the convergence of the fitness function. Differences in the population size primarily affect the decline rate of the fitness function, but it does not show observable regularity. When the population size is 60, the function value at the early stage of evolution declines at the fastest rate, and it converges to the minimum at the 94th generation. Meanwhile, the fitness functions of other population sizes converge around the 100th generation. At the

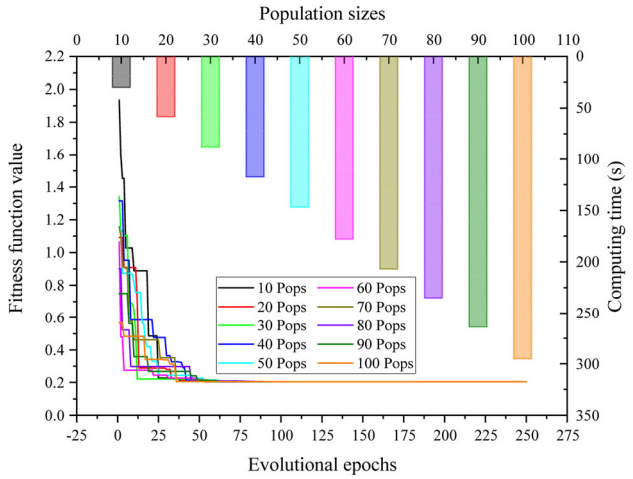

Fig. 16 Effect of different population sizes on the convergence of the fitness function.

same time, the increase in the population size will lead to a linear increase in the calculation time. As illustrated in Fig. 17, the relative errors of the mean thickness for different population sizes are all less than 1%. When a population size increases to 30, the SD of the inversion thickness has a significantly decreasing trend, and the SD is the smallest, which is 49 μm. However, the relative error of the mean thickness is slightly larger than in other cases. When the population size is 40, the mean thickness is closer to the true value, with a SD of 69 μm, and the repeated calculation stability is higher. As the population size increases, the SD also increases and ultimately fluctuates around 90 μm. Therefore, considering the mean thickness, SD, calculation time, and calculation stability, the population size of 40 is selected as the optimal algorithm parameter.

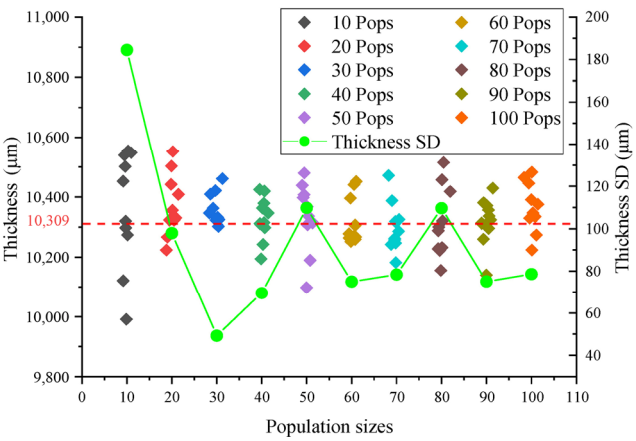

Fig. 17 Effect of different population sizes on thickness inversion results.

4 Experimental apparatus

4.1 Wear measuring system

As shown in Fig. 18, the wear test system of this experiment consisted of a delay block probe, a pulse generator, a digital oscilloscope, and a high precision spiral micrometer. The delay block probe is manufactured by BIGPROBE, which uses a 13 mm diameter composite chip with a center frequency of 2.25 MHz. The delay block material is polymethyl methacrylate (PMMA) with a thickness of 15 mm and an acoustic impedance of $3.29{\cdot}10^5$ g·cm^{-2}·s^{-1}. Additionally, the pulse generator model is Olympus 5072PR, which can generate negative spike pulses with a bandwidth of 35 MHz (–3 dB) and a maximum repetition frequency of 5 kHz. It has both the ultrasonic echo mode and ultrasonic transmission mode and can perform 1 MHz high-pass filtering and 10 MHz low-pass filtering. Also, the digital oscilloscope is used to receive pulse-echo RF signals, and the model is RIGOL DS2102A with dual-channel input display, a bandwidth of 100 MHz, and a maximum sampling frequency of 2 GSa·s^{-1}. The acquired initial time-domain waveform of the probe is presented in Fig. 19. Its –6 dB effective bandwidth of frequency-domain is 1.87–3.01 MHz. The high-precision spiral micrometer is employed for thickness calibration with a resolution of 1 μm and an accuracy of ± 2 μm. Currently, the resolution of the entire measuring system is 50–100 μm.

4.2 Test bench and objects

As shown in Fig. 20, the test bench is composed of an inverter motor, a torque meter, a test chamber, a loading module, and a lubrication module. Moreover, the

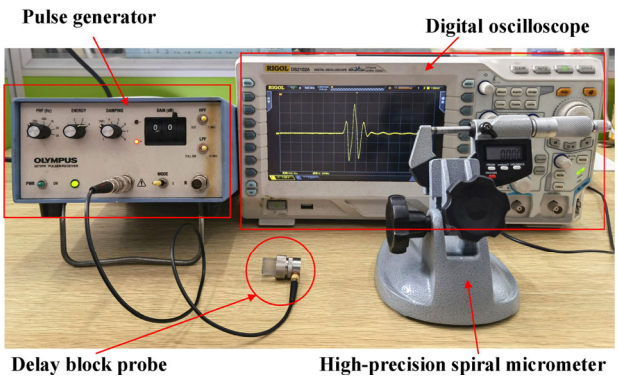

Fig. 18 Wear measuring system.

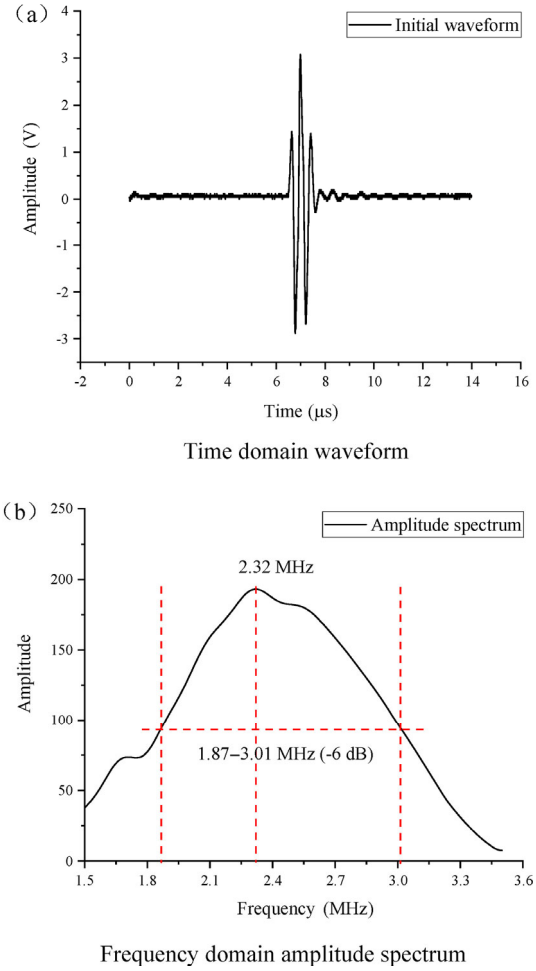

Fig. 19 Initial waveform of 2.25 MHz probe.

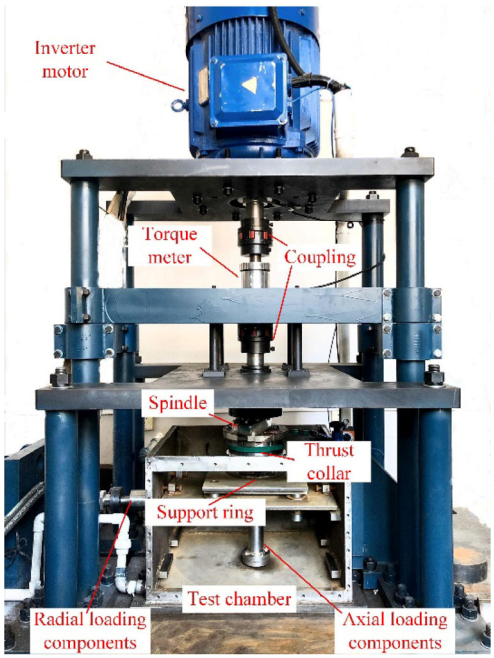

Fig. 20 Vertical bearing test bench.

rated power of the motor is 37 kW, with a speed range of 10–1,500 r·min^{-1}, and the rated torque is 220 N·m. The test bearing is installed in the test chamber, and the modular installation scheme is adopted, which can perform radial bearings, thrust bearings, and radial-thrust bearing experiments. The test bench can install thrust bearings with a maximum outer diameter of 450 mm or radial bearings with a maximum inner diameter of 200 mm. Subsequently, the loading module utilizes a hydraulic loading scheme, which can achieve the static axial load of 30 kN, the dynamic axial load of 6 kN, the static radial load of 20 kN, and the dynamic radial load of 4 kN. The water tank of the lubrication module has a heating function, which can simulate seawater and sediment water, and the flow range of the circulating water pump is 0–60 L·min^{-1}.

Figure 21 shows the test bearing and thrust collar. To compare them with the traditional ultrasonic method, the homogeneous polymer material PEEK is selected to create two fixed pad bearings, with an inner diameter of 124 mm, an outer diameter of 196 mm, and a cover angle of 30°. Regarding the thickness of the pads, #1 is 10,309 μm, and #2 is 10,299 μm. Both the front and back sides are polished, and the surface roughness is approximately 1 μm. The density of PEEK is measured according to the mass and volume of the pad, and the acoustic velocity is calculated according to Eq. (13). The stainless-steel thrust collar has an inner diameter of 124 mm and an outer diameter of 200 mm. Its surface is polished with 2,000 grit sandpaper. Upon installation and calibration, the working surface has a rotation runout error of 0.05 mm. Table 1 itemizes the physical parameters of the two.

Table 1 Physical parameters of PEEK and stainless-steel.

Parameter	PEEK	Stainless-steel
Density (kg·m^{-3})	1,270	7,900
Elastic modulus (GPa)	3.8	194
Poisson's ratio	0.4	0.29
Longitudinal wave velocity (m·s^{-1})	2,532	5,640
Acoustic impedance (g·cm^{-2}·s^{-1})	3.22×10^{5}	4.46×10^{6}

4.3 Test conditions and methods

As shown in Fig. 22, to verify the accuracy of the ultrasonic wear test method, the thrust bearing heavy load accelerated wear test was carried out for a total of 10 h with a constant speed of 500 r·min^{-1}. Before the test, two pads were immersed in water for 48 h at room temperature, and the thickness change was less than 2 μm. The first two hours were the commissioning and running-in stage. Then, the load was set to 0.5 MPa to start the formal test for six hours. For the last two hours, the load was gradually reduced. In order to avoid the influence of pressure, temperature, and other factors on the thickness of the pads, which were disassembled every hour for thickness calibration, and the thickness at the center of the bearing was measured and recorded by the ultrasonic measuring system and the high-precision spiral micrometer, respectively. Next, the test signal was imported into the inversion calculation program. Subsequently, the Fourier transform of the time-domain echo signal was executed to obtain the effective frequency band amplitude spectrum, and then the measured URCAS was derived. According to the theoretical URCAS, the objective function was constructed and substituted

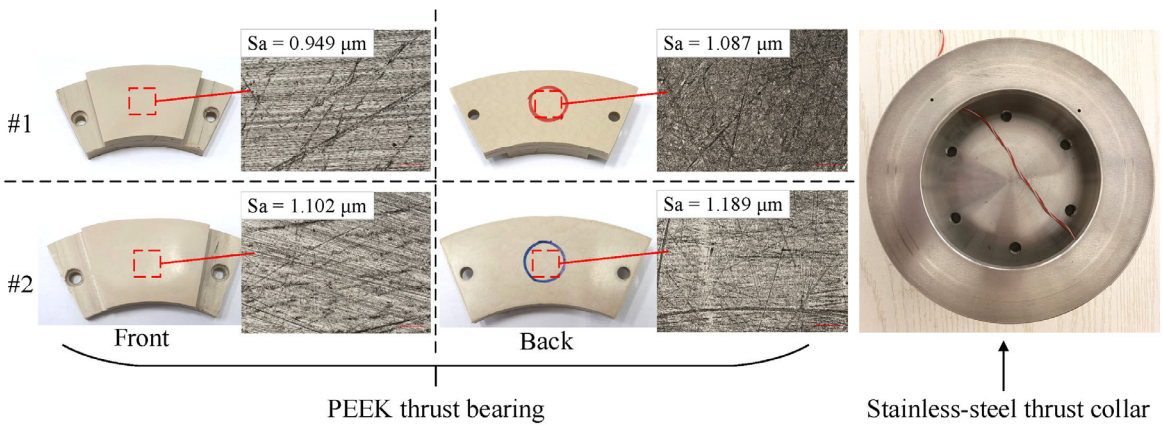

Fig. 21 Test bearings and thrust collar.

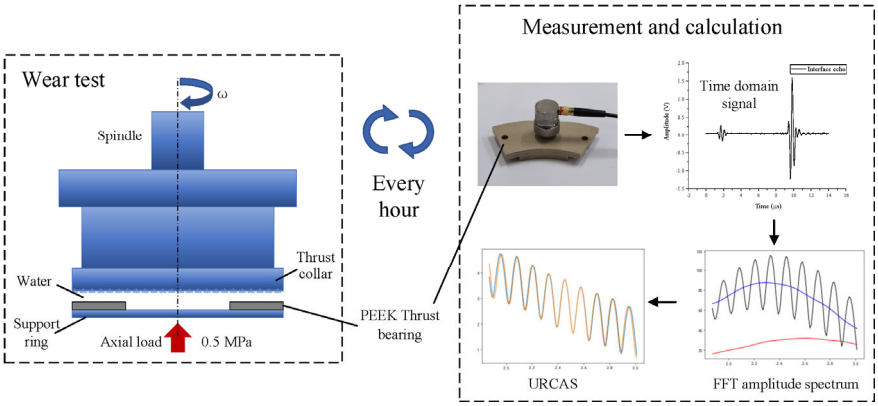

Fig. 22 Test scheme for wear measurement of the bearings.

into the DEA for global optimization. Ultimately, the most matching thickness parameter was identified.

5 Results and discussion

The surface morphology of the bearing after wear is presented in Fig. 23. On the surface of the #1 pad, obvious furrow-like wear marks caused by abrasive wear can be seen, and the surface roughness increases by 0.106 μm. In addition to furrow wear marks, there are many small pits caused by adhesive wear and some oblique scratches on the surface of the #2 pad, which may be caused by generated abrasive particles or impurities, and the surface roughness increases by 0.118 μm.

5.1 Identification results for different ultrasonic methods

Figure 24(a) shows the identification results of the thickness and relative error (E_r) of the #1 pad. After

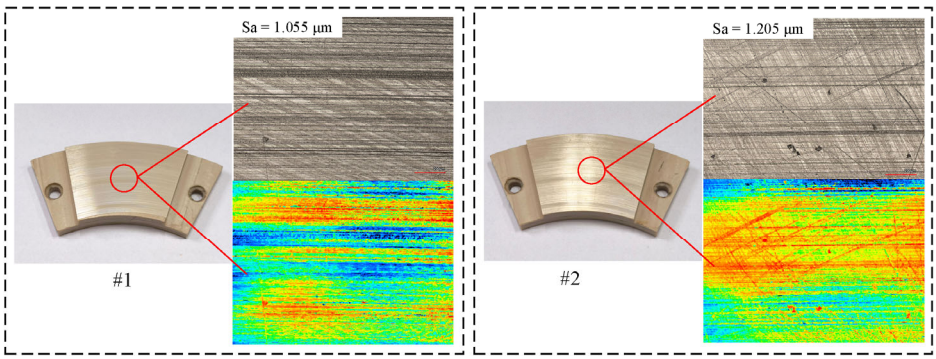

Fig. 23 Surface morphology of the bearings after wear.

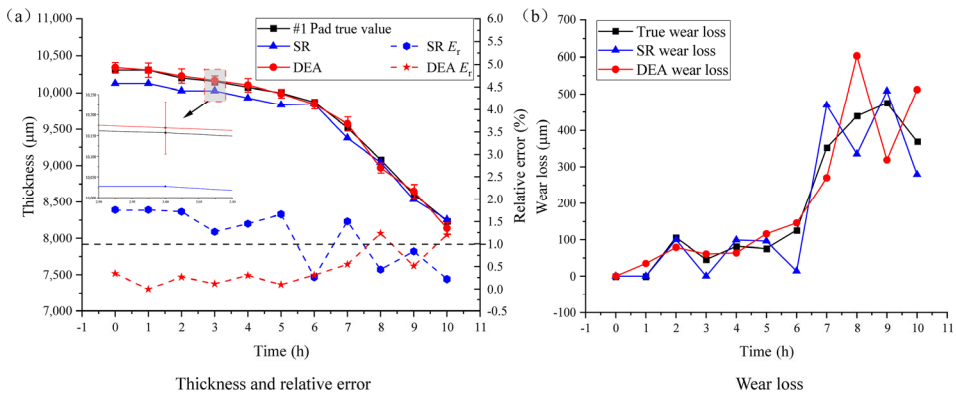

Fig. 24 Identification results of different ultrasonic methods of the #1 pad.

10 h of wear, the thickness of the pad is reduced by 2,071 μm. The identification result of DEA method is the closest to the true value, and the maximum relative errors is 1.23%. The relative error of the SR method is relatively large in the previous calculation, and the maximum is 1.76%. The SR methods rely on accurate prior knowledge of acoustic velocity, which is calculated from the precise density, elastic modulus, and Poisson's ratio. However, DEA method's advantage is that it does not require prior knowledge of acoustic velocity and can dynamically identify the parameter changes of the medium. During the operation process, the acoustic velocity of PEEK will decrease along with the increase in temperature, which the traditional method is unable to measure accurately. As shown in Fig. 24(b), the wear amount of the bearing increases gradually with time until the load is reduced to 0.4 and 0.3 MPa in the last two hours, respectively, and the increasing trend of the wear amount is slowed down. The maximum wear amount is 475 μm at 9 h. The difference between the wear amount identified through the DEA method and the true value is small in the 0–7 h. Eventually, the error becomes larger, which may be related to the surface morphology of the bearing after wear. Overall, the SR method is relatively inaccurate.

Figure 25(a) is the identification results of the thickness and relative error of the #2 pad. After the test, the thickness of the pad is reduced by 1,557 μm, which is 514 μm less than the overall wear of the #1 pad, indicating that the thrust collar is tilted towards the direction of the #1 during the operation process. The identification result of DEA method is the closest to the true value, and the overall relative errors are both less than 1%, of which the maximum errors is 0.66%. The overall relative error of the SR method is large, floating above and below 1%, and the maximum is 1.78%. The thickness SD of the two pads using the DEA method is less than 100 μm. As presented in Fig. 25(b), the wear amount of the bearing increases gradually with time. At the 9th h, the load is reduced to 0.4 MPa, and the wear amount remains significantly increased to the maximum at 430 μm. Then, the load is reduced to 0.3 MPa at the final hour, and the wear amount is reduced to 369 μm. The health state of the bearing is gradually deteriorating during the test. Among them, the DEA method is more accurate, while the fluctuation of the SR method is relatively large.

5.2 Identification results of different intelligent algorithms

In order to discuss the difference of various intelligent algorithms in the thickness identification of polymer bearings, the widely used genetic algorithm (GA) and particle swarm optimization (PSO) algorithm are selected for comparison. The evolution epochs and population size are kept consistent with DEA in the algorithm parameters. Figure 26(a) is the thickness identification results of the #1 pad. The errors of the three algorithms are relatively close, and there is a gradually increasing trend with the test, which may be related to the change in the bearing surface morphology. Among them, the error fluctuation of

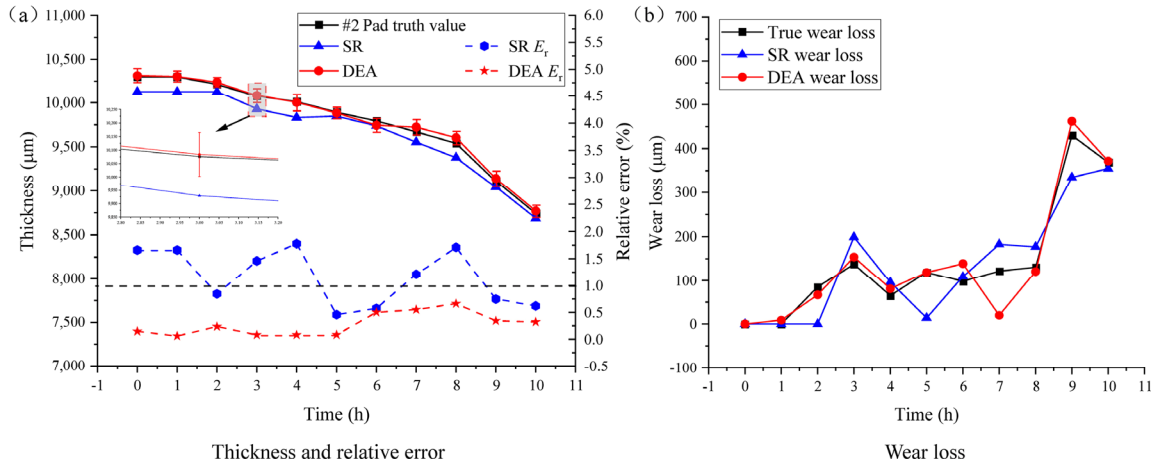

Fig. 25 Identification results of different ultrasonic methods of the #2 pad.

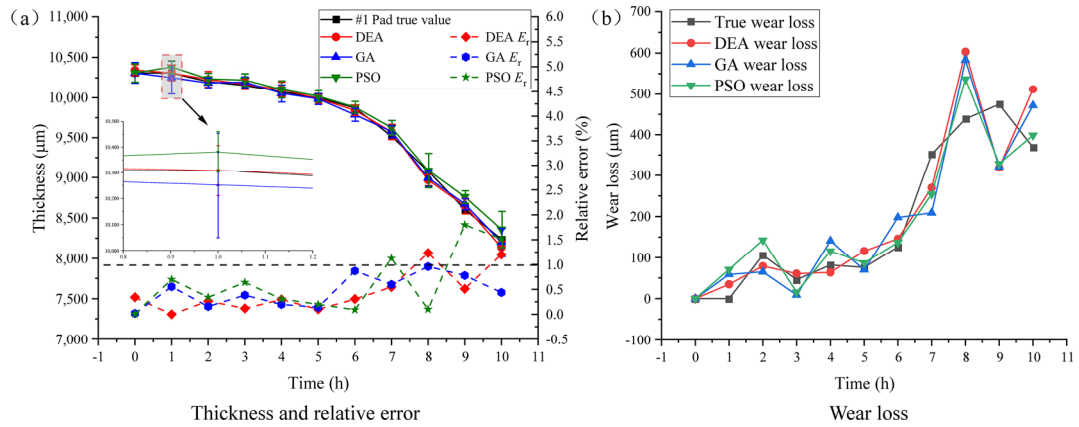

Fig. 26 Identification results of different intelligent algorithms of the #1 pad.

PSO is larger, and the maximum error is 1.8%. The relative error of the GA is less than 1%. Combined with the local amplification diagram, the error band of GA and PSO is larger, and the maximum is 224 μm. In addition, the relative error of DEA is similar to GA, and the error band is less than 100 μm, indicating that the stability of DEA is better, since it is essentially an improved GA that ensures the calculation error and improves the stability. As shown in Fig. 26(b), DEA is the most accurate to identify the wear amount in 0–7 h, and the latter three algorithms cannot accurately reflect the trend of wear amount. The analysis highlights that the change of roughness at the bearing measuring point leads to an increase in the algorithm identification error.

Figure 27(a) shows the thickness identification results of the #2 pad. The calculation error of DEA is the smallest, amounting to about 0.5% as a whole. At the 6th h, the error of GA only exceeds 1%–1.5%. Then, from the 7th h, the error of PSO increases, and the maximum is 2.2%. Combined with the local amplification diagram, it can also be found that the error band fluctuation of GA and PSO is larger than that of DEA, and the maximum is 219 μm. At the same time, the error band of DEA is less than 100 μm. This conclusion is consistent with that of the #1 pad. As illustrated in Fig. 27(b), DEA is more accurate in the identification of wear. Compared with GA and PSO, the three algorithms have larger errors in the 7th h. The analysis finds that it may be the error caused by the change in the surface morphology of the measuring point. Therefore, based on the identification results of two pads and three algorithms, DEA is superior to the widely used GA and PSO with smaller error and higher stability.

In order to validate the test accuracy of the proposed method, this paper adopts an off-line *non-in-situ* measurement and compares the thickness calibration

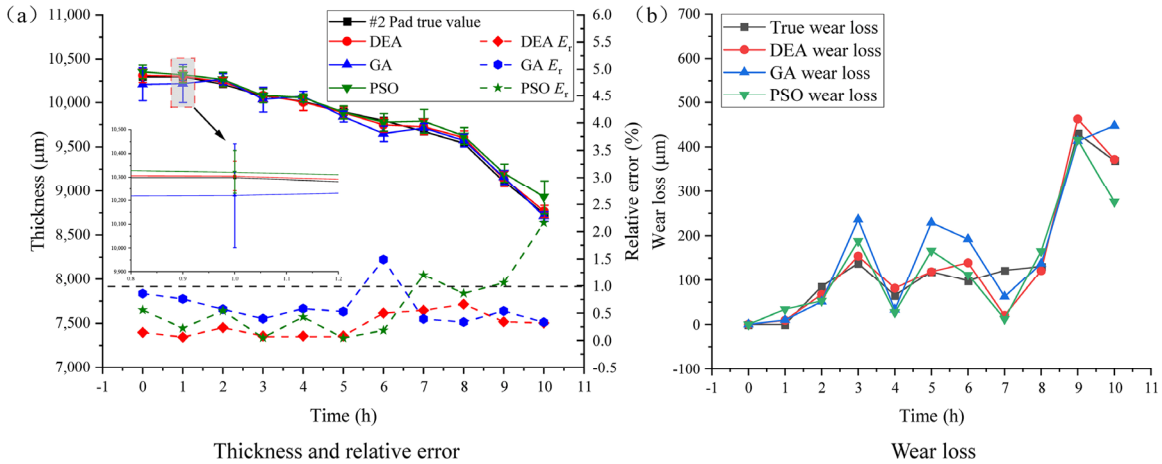

Fig. 27 Identification results of different intelligent algorithms of the #2 pad.

results of the high-precision spiral micrometer. The error of PEEK thickness identification is fundamentally 1% without prior knowledge, but the deficiency is that a complete *in-situ* on-line monitoring system has not been formed at present, which requires further research.

6 Conclusions

1) A wear monitoring method of polymer bearing based on ultrasonic reflection coefficient amplitude spectrum (URCAS) is proposed, which combines the intelligent algorithm to transform the parameter inversion problem into an extremum optimization problem. Then, it simultaneously solves the four parameters of the bearing's sound velocity, density, thickness, and attenuation factor. It addresses the problem caused by the difficulty involved in accurately obtaining the physical and geometric parameters of polymer materials, which have values that are variable.

2) The influence of bearing parameters, objective function, and algorithm parameters on the identification results is simulated and analyzed. The 10% increase or decrease of acoustic velocity and thickness will result in a large degree of deviation of the URCAS. The correlation coefficient decreases to 0.75–0.85, and the root mean square error increases to 0.88–1.04. The 10% increase in density has a greater influence than that of the 10% decrease in density. Equally important, the increase or decrease in attenuation factor will only lead to the increase in root mean square error. In short, to ensure that the inversion errors of the bearing parameters are less than 10%, the correlation coefficient needs to be greater than 0.991, and the root mean square error is less than 0.411. The correlation coefficient, root mean square error, and the combination of the two are selected as the objective functions of the intelligent algorithm. It is found that the identification results using the dual objective functions have higher accuracy than those using the correlation coefficient alone and have a higher concentration than those solely using the root mean square error. Upon the selection of different evolutionary epochs and population size, particularly when the evolutionary epochs are 250 and the population size is 40, the calculation accuracy and time can be considered when the fitness function converges.

3) In order to verify the accuracy of this method with precision measuring tools and traditional ultrasonic methods, the homogeneous polymer material poly-ether-ether-ketone (PEEK) was selected to make bearings, and the accelerated wear test for a total of 10 h was carried out. The results highlight that, without prior knowledge, the proposed method can achieve the high-accuracy in thickness and wear loss identification, which is better than the spectral resonance (SR) method. Through the comparison of various algorithms, this study found that differential evolution algorithm (DEA) has a smaller error and higher stability than genetic algorithm (GA) and is superior to particle swarm optimization (PSO). In this case, the overall error can be maintained at about 1%.

4) The wear amount is the most direct parameter to characterize the bearing life. This paper proposes and verifies the bearing wear identification accuracy of this method under static and offline conditions. Subsequently, an online monitoring system can be built to realize the real-time monitoring of the bearing wear on the test bench, as well as predict the residual life of the bearing. At the same time, the error mechanism and influencing factors of this method are analyzed to augment the test accuracy.

Acknowledgements

This study is supported by the National Key R&D Program of China (No. 2018YFE0197600), the European Union's Horizon 2020 Research and Innovation Programme RISE under Grant Agreement No. 823759 (REMESH), and the National Natural Science Foundation of China (No. 52071244).

References

[1] Orndorff R. Water-lubricated rubber bearings, history and new developments. *Nav Eng J* **97**(7): 39–52 (1985)

[2] Han Y F, Xiong S W, Wang J X, Wang Q J. A new singularity treatment approach for journal-bearing mixed lubrication modeled by the finite difference method with a herringbone mesh. *J Tribol-T ASME* **138**(1): 011704 (2016)

[3] Ouyang W, Zhang X, Jin Y, Yuan X. Experimental study on the dynamic performance of water-lubricated rubber bearings with local contact. *Shock Vib* **2018**: 6309727 (2018)

[4] Litwin W. Influence of local bush wear on water lubricated sliding bearing load carrying capacity. *Tribol Int* **103**: 352–358 (2016)

[5] Fka B, Xza B, Jian H, Hao W B, Pz B. Machine-vision-based assessment of frictional vibration in water-lubricated rubber stern bearings. *Wear* **426**: 760–769 (2019)

[6] Han H, Lee K. Experimental verification of the mechanism on stick–slip nonlinear friction induced vibration and its evaluation method in water-lubricated stern bearing. *Ocean Eng* **182**: 147–161 (2019)

[7] Zhang Z, Zhang Z, Huang X, Hua H. Stability and transient dynamics of a propeller-shaft system as induced by nonlinear friction acting on bearing-shaft contact interface. *J Sound Vib* **333**(12): 2608–2630 (2014)

[8] Huang Q, Yan X, Zhang C, Zhu H. Coupled transverse and torsional vibrations of the marine propeller shaft with multiple impact factors. *Ocean Eng* **178**: 48–58 (2019)

[9] Guo Z, Xie X, Yuan C Q. Study on influence of micro convex textures on tribological performances of UHMWPE material under the water-lubricated conditions. *Wear* **426–427**: 1327–1335 (2019)

[10] Qu J, Truhan J J. An efficient method for accurately determining wear volumes of sliders with non-flat wear scars and compound curvatures. *Wear* **261**(7–8): 848–855 (2006)

[11] Bhushan B, Lowry J A. Friction and wear studies of various head materials and magnetic tapes in a linear mode accelerated test using a new nano-scratch wear measurement technique. *Wear* **190**(1): 1–15 (1995)

[12] Scherge M, PÖhlmann K, A Gervé. Wear measurement using radionuclide-technique (RNT). *Wear* **254**(9): 801–817 (2003)

[13] Sheng C, Wu T, Zhang Y. Non-destructive testing of marine diesel engines using integration of ferrographic analysis and spectrum analysis. *Insight-Non-Destructive Testing and Condition Monitoring* **54**(7): 394–398 (2012)

[14] Jurkovic J, Korosec M, Kopac J. New approach in tool wear measuring technique using CCD vision system. *Int J Mach Tool Manu* **45**(9): 1023–1030 (2005)

[15] Zhang S J, To S, Cheung C F, Du J J. Novel auto-regressive measurement of diamond tool wear in ultra-precision raster milling. *Int J Precis Eng Man* **13**(9): 1661–1670 (2012)

[16] Warner J A, Gladkis L G, Smith P N, Scarvell J M, Timmers H. Demonstration of a new technique using radioisotope tracers to measure the backside wear rate on tibial inserts. *Tribol Lett* **46**(2): 139–145 (2012)

[17] Yuan C Q, Li J, Yan X P, Peng Z. The use of the fractal description to characterize engineering surfaces and wear particles. *Wear* **255**(1–6): 315–326 (2003)

[18] Wang S, Wu T, Wang K, Sarkodie-Gyan T. Ferrograph analysis with improved particle segmentation and classification methods. *J Comput Inf Sci Eng* **20**(2): 1–12 (2019)

[19] Xu X J, Yan X P, Sheng C X, Yuan C Q, Xu D L, Yang J B. A belief rule-based expert system for fault diagnosis of marine diesel engines. *IEEE Trans Syst Man Cybern Syst* **50**(2): 656–672 (2020)

[20] Kang Y, Shi K, Meng Y. Study on wear quantity testing device for extra-large size thrust bearing. *Journal of Harbin Bearing* **4**: 33–35 (2016)

[21] Long M, Rack H. Ultrasonic *in situ* continuous wear measurements of orthopaedic titanium alloys. *Wear* **205**(1–2): 130–136 (1997)

[22] Ahn H, Kim D I. *In situ* evaluation of wear surface by ultrasound. *Wear* **251**(1–12): 1193–1201 (2001)

[23] Abu-Zahra N., Yu G. Gradual wear monitoring of turning inserts using wavelet analysis of ultrasound waves. *Int J Mach Tool Manu* **43**: 337–343 (2003)

[24] Zhao Y, Lin L, Li X M, Lei M K. Simultaneous determination of the coating thickness and its longitudinal velocity by ultrasonic nondestructive method. *Ndt & E Int* **43**(7): 579–585 (2010)

[25] Ma Z Y, Luo Z B, Lin L, Krishnaswamy S, Lei M K. Quantitative characterization of the interfacial roughness and thickness of inhomogeneous coatings based on ultrasonic reflection coefficient phase spectrum. *Ndt & E Int* **102**: 16–25 (2019)

[26] Balasubramaniam K, Rao N S. Inversion of composite material elastic constants from ultrasonic bulk wave phase velocity data using genetic algorithms. *Compos B Eng* **29**(2): 171–180 (1998)

[27] Storn R, Price K. Differential evolution—A simple and efficient heuristic for global optimization over continuous spaces. *J Global Optim* **11**(4): 341–359 (1997)

Changxiong NING. He received his bachelor degree in marine engineering in 2018 from Wuhan University of Technology, Wuhan, China. Then he has been a Ph.D. student in the National Engineering Research Center for Water Transport Safety at the same university. His research interests include rim-driven thruster intelligent maintenance and health management.

Xinping YAN. He received his Ph.D. degree in mechanical engineering from Xi'an Jiaotong University, Xi'an, China, in 1997. He is an academician of the Chinese Academy of Engineering. His current position is a professor and the director of the National Engineering Research Center for Water Transport Safety, Wuhan University of Technology. He is committed to the research on safety, intelligence, and green technology of transportation system.

Wu OUYANG. He received his Ph.D. degree in mechanical engineering from Xi'an Jiaotong University, Xi'an, China, in 2014. He is a professor of the National Engineering Research Center for Water Transport Safety, Wuhan University of Technology. His research areas cover the green and efficient propulsion technology, and friction and lubrication technology of propulsion system.